Fluid Exchange across a Meandering Jet with Quasiperiodic Variability

JINQIAO DUAN

Applied Mechanics, California Institute of Technology, Pasadena, California

STEPHEN WIGGINS

Applied Mechanics, and Control and Dynamical Systems, California Institute of Technology, Pasadena, California

(Manuscript received 30 June 1995, in final form 27 October 1995)

ABSTRACT

In this paper, the motion of fluid parcels in the two-dimensional kinematic model of a meandering jet developed by Bower and Samelson is studied. The earlier work is extended by considering quasiperiodic spatiotemporal variability in a reference frame moving with the phase speed of the meander. This necessitates the introduction of recently developed techniques in dynamical systems theory for analyzing transport in velocity fields with quasiperiodic variability.

A detailed comparison between exchange for variability with one and two independent frequencies is given, and it is shown that the exchange rates may be very different for periodic and quasiperiodic variability.

1. Introduction

In this paper we will be concerned with fluid exchange across kinematical models of meandering jets. There have been several studies of such models in the past few years, many of them motivated by the work of Bower (1991). Based on RAFOS float observations of the Gulf Stream, she devised a kinematical model consisting of a jet of uniform width deformed by a steadily propagating sinusoidal meander. In a reference frame moving with the meander the fluid motion is steady and, for eastward meander propagation, consisted of three regimes: a central jet, exterior retrograde motion, and intermediate closed circulations above meander troughs and below crests. Since the fluid motion was steady, no exchange could occur between the three regimes. However, float observations indicate that exchange does occur across some parts of the Gulf Stream. Samelson (1992) recognized that this must be due to deviations from the regular pattern of Bower's model and modified her model to include additional spatiotemporal variability in the velocity field. In particular, he allowed for a time-dependent meander amplitude, a time-dependent spatially uniform meridional velocity superimposed on the basic flow, and a propagating plane wave superimposed on the basic flow. It is important to note that Samelson only considered periodic variability, which resulted in time-periodic velocity fields. This is because time-periodic velocity fields are of the form where the methods and viewpoint of modern dynamical systems theory can be brought to bear on issues related to fluid transport and mixing. To motivate this, we provide some brief background.

Two-dimensional, incompressible, time-dependent velocity fields can be written as follows:

$$\dot{x} = \frac{\partial \psi}{\partial y}(x, y, t),$$

$$\dot{y} = -\frac{\partial \psi}{\partial x}(x, y, t), \tag{1}$$

where $\psi(x, y, t)$ is the streamfunction. These equations also describe the evolution of fluid particle trajectories. From the point of view of a dynamical systems theorist, (1) are just Hamilton's canonical equations where the streamfunction plays the role of the Hamiltonian function and the phase space is just the physical space of the fluid flow. If the flow is time periodic, then the study of (1) is typically reduced to the study of a two-dimensional *Poincaré map*. Practically speaking, this means that rather than viewing a particle trajectory as a curve in continuous time, one views the trajectory only at discrete intervals of time, where the interval of time is the period of the velocity field. The value of making this analogy with Hamiltonian dynamical systems lies in the fact that a variety of techniques in this area have immediate applications to, and implications for, transport and mixing processes in fluid mechanics. For example, the persistence of invariant curves in the

Corresponding author address: Dr. Stephen Wiggins, Applied Mechanics, and Control and Dynamical Systems, Division of Engineering and Applied Science 104-44, California Institute of Technology, Pasadena, CA 91125.
E-mail: wiggins@chaos.thomas.caltech.edu

Poincaré map (KAM curves) gives rise to barriers to transport; chaos and Smale horseshoes provide mechanisms for the "randomization" of fluid particle trajectories; Melnikov's method allows one to analytically estimate fluxes as well as describe the parameter regimes where chaotic fluid particle motions occur; lobe dynamics enables one to efficiently compute transport between qualitatively different flow regimes; bifurcation theory enables one to understand how qualitatively different flow regimes appear and disappear as system parameters are varied; etc. In short, many new methods for the study of fluid transport and mixing can be obtained from dynamical systems theory. For a survey of this from the dynamical systems viewpoint see Wiggins (1992) and Beigie et al. (1994), and for a survey from the fluid mechanics viewpoint see Ottino (1989).

Traditionally, the mathematical development of Hamiltonian dynamical systems theory has been in the context of discrete time (or maps) or for continuous time where the time dependence is either steady or periodic. In recent years, many of the techniques described above have been extended to the situation where the time dependence is more general than periodic; however, these techniques have been slow in making their way into the applied community. In this paper will reconsider Samelson's model of a meandering jet, but we will allow for more general spatiotemporal variability than time periodicity.

The situation of temporal variability that is more general than periodic has not received much attention. One of the obstructions is that for two-dimensional, temporally *nonperiodic* velocity fields there is no reduction to a two-dimensional Poincaré map in the sense that trajectories of the Poincaré map are interpolated by the continuous time trajectories of the flow. The significance of this is that many of the relevant results of dynamical systems theory—the KAM theorem, the Smale horseshoe construction, Melnikov's method—were originally developed in the context of two-dimensional maps or two-dimensional time-periodic vector fields. However, in the past few years many of these results relevant to transport have been generalized to the case of time *quasiperiodic* variability, that is, the case where the variability has a finite number of independent and possibly incommensurate frequencies; see Beigie et al. (1991, 1992) and Wiggins (1992). The mathematical theory is significantly more involved than for the case of time-periodic variability. However, the general spirit and elements behind the analysis remain essentially the same. Namely, the mathematical results and techniques allow one to understand, and deal with, saddle-type stagnation points that oscillate quasiperiodically in time. These oscillating stagnation points have stable and unstable manifolds that have the same significance for fluid parcel transport. That is, at each instant of time they form boundaries in the flow between parcel trajectories that move in different directions after their encounter with the quasiperiodically oscillating stagnation point. However, there is a very significant difference with the case of time-periodic variability. Namely, in that case there is a distinguished interval of time: the period, after which the velocity field returns to its same values at each point in the flow. As a result, when considering parcel trajectories via the Poincaré map, the stable and unstable manifolds are *fixed curves in space.* In this situation intuition derived from the kinematics of two-dimensional steady flows is useful (since in that case streamlines are fixed curves in space), provided we make the correct interpretation of the kinematics of the trajectories of the Poincaré map (which are infinite sequences of discrete points) in terms of parcel trajectories for the unsteady, time-periodic flow. In the case of quasiperiodically time varying velocity fields, there is no way to avoid the fact that the stable and unstable manifolds vary in time, and consequently we must deal with the problem of *transport across a moving curve.* This has the immediate implication that, even though the flow is incompressible, the *instantaneous flux* in one direction across such a moving curve may not equal the instantaneous flux in the opposite direction. We will see that this does have physical consequences for finite time transport.

2. Derivation of the model

We briefly describe the model of the meandering jet studied by Bower (1991) and Samelson (1992), and we follow the notation of this latter reference as closely as possible.

The streamfunction for the basic meandering jet has the form

$$\psi(x', y, t) = \psi_0\left[1 - \tanh\left(\frac{y - A\cos k(x' - c_x t)}{\lambda[1 + k^2A^2\sin^2 k(x' - c_x t)]^{1/2}}\right)\right], \tag{2}$$

where x' and y are Cartesian coordinates indicating positive eastward and northward, respectively, $2\psi_0$ is referred to as the total eastward transport, λ determines the width of the jet, and A, k, and c_x are respectively the amplitude, wavenumber, and phase speed of the meander. A frame of reference moving with the meander is given by

$$X = x' - c_x t, \quad Y = y, \tag{3}$$

and in this frame the streamfunction, after nondimensionalization, takes the form

$$\phi(\xi, \eta) = 1 - \tanh\left[\frac{\eta - B\cos\kappa\xi}{(1 + \kappa^2B^2\sin^2\kappa\xi)^{1/2}}\right] + c\eta, \tag{4}$$

where

$$\phi = \psi_0^{-1}\psi + c\eta, \quad (\xi, \eta) = \lambda^{-1}(X, Y), \quad B = \lambda^{-1}A,$$
$$\kappa = 2\pi\mathrm{L}^{-1} = k\lambda, \quad c = \lambda\psi_0^{-1}c_x,$$

and the dimensionless time and length are given by

$$\tau = \psi_0 \lambda^{-2} t, \quad x = \lambda^{-1} x'.$$

Streamlines of the steady flow

Following Samelson (1992), we will fix the parameters for the basic meandering jet at the following values:

$$B = 1.2, \quad L = \frac{2\pi}{\kappa} = 10, \quad c = 0.1.$$

The streamlines in the moving frame for these parameter values are shown in Fig. 1 of Samelson (1992). We sketch the separatrices that define the qualitatively distinct regimes of fluid parcel motion in Fig. 1.

In Fig. 1 we sketch only the separatrices associated with the jet in the moving frame, and we see that there are three distinct types of fluid parcel trajectories—eastward moving parcels in the jet, westward moving parcels exterior to the jet, and parcels that execute periodic trajectories. These three types of trajectories exist in five distinct regions whose boundaries consist of separatrices connecting saddle-type stagnation points. In the figure the regions bounded by the separatrices are denoted by R_i, $i = 1, \cdots, 5$. Since the flow is steady in the moving frame, no exchange between these regions can occur in the moving frame. Hence, no transport of fluid parcels into or out of the jet can occur in the moving frame.

3. Exchange due to quasiperiodic variability in the moving frame: A comparison with periodic variability

Samelson (1992) considers three types of variability in the moving frame: a periodically varying meander amplitude, a superimposed periodically time-varying spatially uniform meridional flow, and a superimposed propagating wave train. We will consider exactly the same forms for the variability, but instead we will allow them to vary quasiperiodically in time. With this variability Samelson considers exchange between the northern recirculation cell and the northern retrograde region (R_1 and R_2 in our notation) and exchange between the jet core (R_3) and the northern recirculation cell (R_2). We will consider the same exchange problems. By symmetry, exchange between R_4 and R_5 is the same as that between R_1 and R_2, and exchange between R_3 and R_4 is the same as that between R_2 and R_3.

a. Quasiperiodically time-varying meander amplitude

Following Samelson (1992), we allow the meander amplitude to vary in time by letting B in (4) have the following form:

$$B = B_0 + \epsilon \sum_{i=1}^{l} \gamma_i \cos(\omega_i \tau + \delta_i). \tag{5}$$

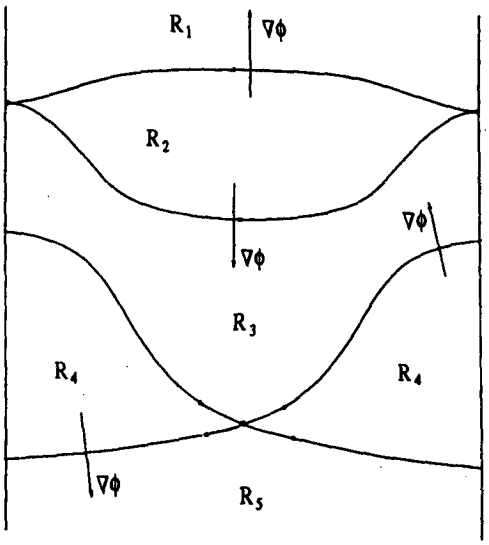

FIG. 1. Separatrices associated with the steady jet in the moving frame.

Substituting this expression into (4) and Taylor expanding in ϵ gives

$$\Phi(\xi, \eta, B) = \phi(\xi, \eta, B_0) + \epsilon \phi'(\xi, \eta, \tau) + O(\epsilon^2), \tag{6}$$

where

$$\phi'(\xi, \eta, \tau) = \frac{\partial \phi}{\partial B}(\xi, \eta, B_0) \sum_{i=1}^{l} \gamma_i \cos(\omega_i \tau + \delta_i).$$

For this streamfunction the quasiperiodic Melnikov functions can now be computed, and this is done in appendix B. With the quasiperiodic Melnikov function in hand, fluxes can then be computed as described in appendix A. Here we describe the results.

1) PERIODIC VARIABILITY

In the case of periodic variability studied by Samelson (1992), he noted that the maximal flux between R_1 and R_2 occurs when the frequency of the variability, ω, is about 0.035, while the maximal flux between R_2 and R_3 occurs when ω is about 0.35. The maximal flux between R_2 and R_3 is about eight times larger than the maximal flux between R_1 and R_2. The most striking feature is the relative difference in the strength of the exchange across the two boundaries. For $\omega = 0.35$ the exchange between R_2 and R_3 is much stronger than the exchange between R_1 and R_2. However, for ω near 0.035, the flux between R_1 and R_2 is about twice the value of the flux between R_2 and R_3.

2) QUASIPERIODIC VARIABILITY, AND THE COMPARISON WITH PERIODIC VARIABILITY

For simplicity we only consider the two-frequency case (i.e., $l = 2$). First, we will consider some transport

issues related to the finite-time average flux. In Fig. 2 we plot the finite-time average flux from R_1 into R_2, $\langle \Phi_{1,2} \rangle_n$, and the finite-time average flux from R_2 into R_1, $\langle \Phi_{2,1} \rangle_n$, up to $n = 20$ nondimensional periods corresponding to ω_2 for the parameter values given in the figure caption. In Fig. 3 we plot the finite-time average flux from R_2 into R_3, $\langle \Phi_{2,3} \rangle_n$ and the finite-time average flux from R_3 into R_2, $\langle \Phi_{3,2} \rangle_n$. Note that all parameters are the same in these two figures *except the frequencies.*

From these figures we easily see that when ω_1 and ω_2 are near the "peak" frequency 0.035 for single frequency variability, the finite-time average flux from R_1 into R_2, $\langle \Phi_{1,2} \rangle_n$, is larger than the finite-time average flux from R_2 into R_3, $\langle \Phi_{2,3} \rangle_n$, when ω_1 and ω_2 are near the corresponding "peak" frequency. Thus, at least for finite times, the situation is the opposite of that observed for the case of single frequency variability described above.

In Fig. 4 we plot $\langle \Phi_{2,3} \rangle_n$ and $\langle \Phi_{3,2} \rangle_n$ for different frequencies than those in Fig. 3, but with *all other parameters unchanged.* In comparing these two figures we see that the finite-time average fluxes in the former case are larger than the latter case. If we were to consider the case of single frequency variability with the size of the frequency roughly the size of one of the frequencies for the case shown in Fig. 4, the flux would decrease

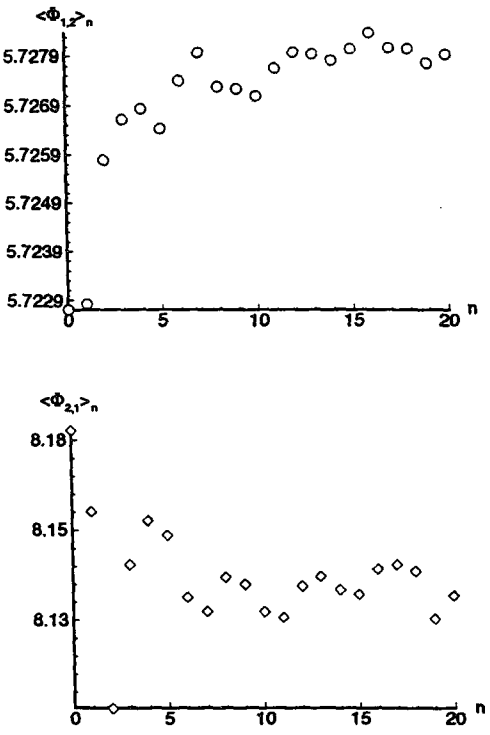

FIG. 2. Finite-time flux between R_1 and R_2; $\omega_1 = 0.01$, $\omega_2 = (\sqrt{2} - 1)/10$, $\delta_1 = 6.25$, $\delta_{20} = \pi$. The amplitudes satisfy $\gamma_1^2 + \gamma_2^2 = 1$ with $\gamma_1 = 0.3$.

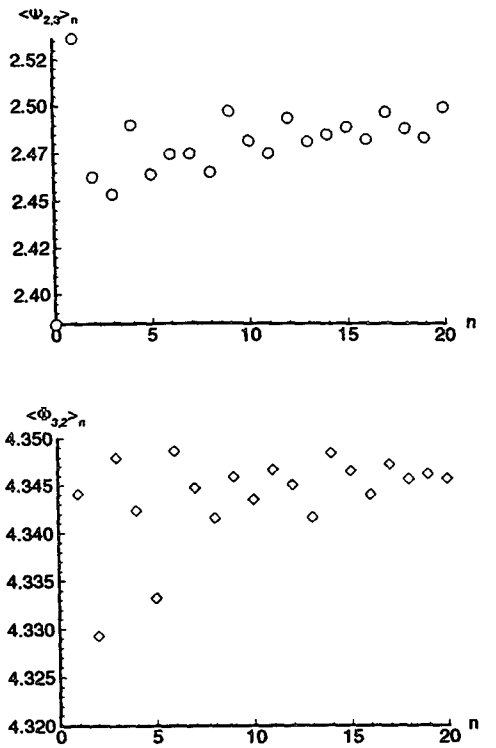

FIG. 3. Finite-time flux between R_2 and R_3; $\omega_1 = \pi/10$, $\omega_2 = 0.5$, $\delta_1 = 6.25$, $\delta_{20} = \pi$. The amplitudes satisfy $\gamma_1^2 + \gamma_2^2 = 1$ with $\gamma_1 = 0.3$.

by at least a factor of $1/2$ in comparison with the maximal flux at $\omega = 0.35$ (cf. Samelson 1992, Fig. 7). The point to be made here is that in the multifrequency case the finite-time average flux may remain relatively large for choices of frequencies that, individually, would result in much smaller fluxes in the corresponding single frequency case.

Note that generally $\langle \Phi_{3,2} \rangle_n \neq \langle \Phi_{2,3} \rangle_n$ and $\langle \Phi_{1,2} \rangle_n \neq \langle \Phi_{2,1} \rangle_n$, which would not be true for periodic variability.

Next we consider the infinite-time average flux. In particular, we want to consider again two-frequency variability and compare the infinite-time average flux in this case with the "single frequency limits." This is done by choosing the normalization $\gamma_1^2 + \gamma_2^2 = 1$ for the amplitude of the variability, fixing ω_1, and then plotting the infinite-time average flux as a function of γ_1 and ω_2. Thus, $\gamma_1 = 0$ corresponds to single frequency variability with frequency ω_2 and $\gamma_2 = 0$ corresponds to single frequency variability with frequency ω_1. For $\omega_1 = 0.02$ we plot $\Phi = \langle \Phi_{1,2} \rangle = \langle \Phi_{2,1} \rangle$, and $\Phi = \langle \Phi_{2,3} \rangle = \langle \Phi_{3,2} \rangle$, respectively, as a function of γ_1 in Fig. 5. From these figures we see that for some nonzero γ_1, γ_2, and ω_2, the infinite-time average flux between R_2 and R_3 can be larger than or comparable with the infinite-time average flux between R_1 and R_2 for sizes of frequencies for which, if taken individually, the op-

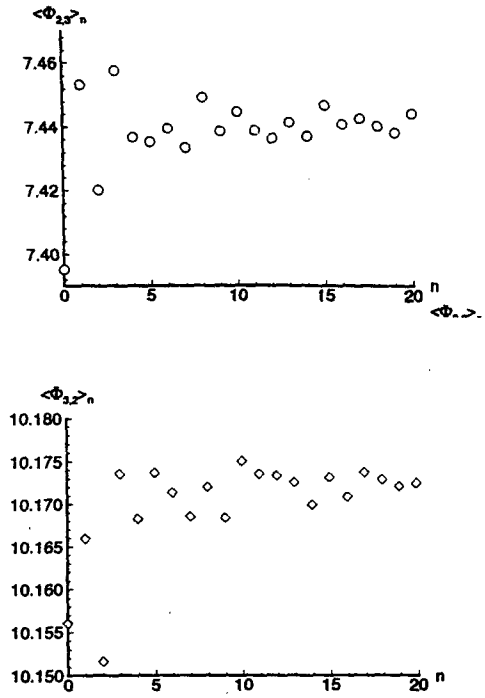

FIG. 4. Finite-time flux between R_2 and R_3; $\omega_1 = 0.12$, $\omega_2 = (\sqrt{2} - 1)/2$, $\delta_1 = 6.25$, $\delta_{20} = \pi$. The amplitudes satisfy $\gamma_1^2 + \gamma_2^2 = 1$ with $\gamma_1 = 0.3$.

posite situation would occur in the corresponding single-frequency case (cf. Samelson 1992, Fig. 7). Hence, we conclude that the addition of more frequency components in the variability may either enhance or suppress exchange as compared with the single frequency case.

To check the global dependence of the infinite-time flux on the two frequencies, we generate a three-dimensional plot of the flux with the other parameters fixed; see Fig. 6. We note that the difference between the maximal flux crossing the two boundaries is increased (comparing with Fig. 7 in Samelson 1992). It appears that the global impact of two-frequency interference is to increase the maximal efficiency of transport across the boundary between R_2 and R_3 and to decrease the maximal efficiency of transport across the boundary between R_1 and R_2.

b. *A superimposed quasiperiodically time-varying spatially uniform meridional flow*

Following Samelson (1992), the nondimensional streamfunction for the spatially uniform meridional flow is of the form

$$\phi'(\xi, \eta, \tau) = \xi \sum_{i=1}^{l} \gamma_i \cos(\omega_i \tau + \delta_i). \qquad (7)$$

1) PERIODIC VARIABILITY

Samelson (1992) found that for periodic variability of this type exchange across the boundary between R_2 and R_3 was always larger than exchange across the boundary between R_1 and R_2 (cf. Fig. 4 from Samelson 1992).

2) QUASIPERIODIC VARIABILITY AND THE COMPARISON WITH PERIODIC VARIABILITY

For quasiperiodic variability with two frequencies, the opposite situation can happen as compared with the single-frequency case.

For some values of parameters, the fluxes crossing the boundary between R_2 and R_3 are smaller than those crossing the boundary between R_1 and R_2. For example, in Figs. 7 and 8 we plot the finite-time average flux for $\omega_1 = 0.3$, $\omega_2 = \pi$, $\gamma_1^2 + \gamma_2^2 = 1$ with $\gamma_1 = 0.5$, $\delta_1 = 3.5$, $\delta_{20} = \pi$. The values of $\langle \Phi_{2,1} \rangle_n$ are smaller than those of $\langle \Phi_{3,2} \rangle_n$.

The global impact of two-frequency interference is evident or strong only for small frequencies. As a function of the two frequencies ω_1 and ω_2, the infinite-time

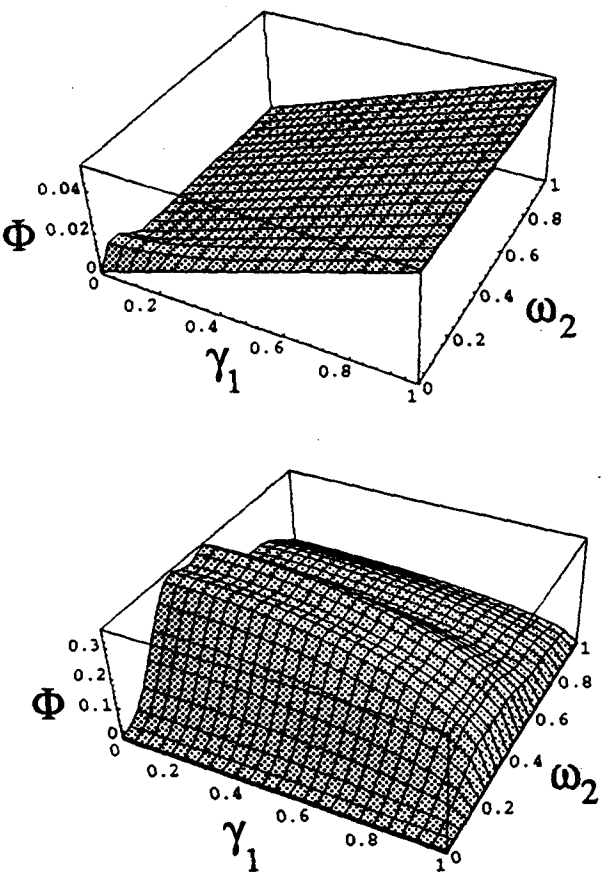

FIG. 5. Infinite-time flux between R_1 and R_2 and between R_2 and R_3, respectively; $\omega_1 = 0.02$, $\gamma_1^2 + \gamma_2^2 = 1$.

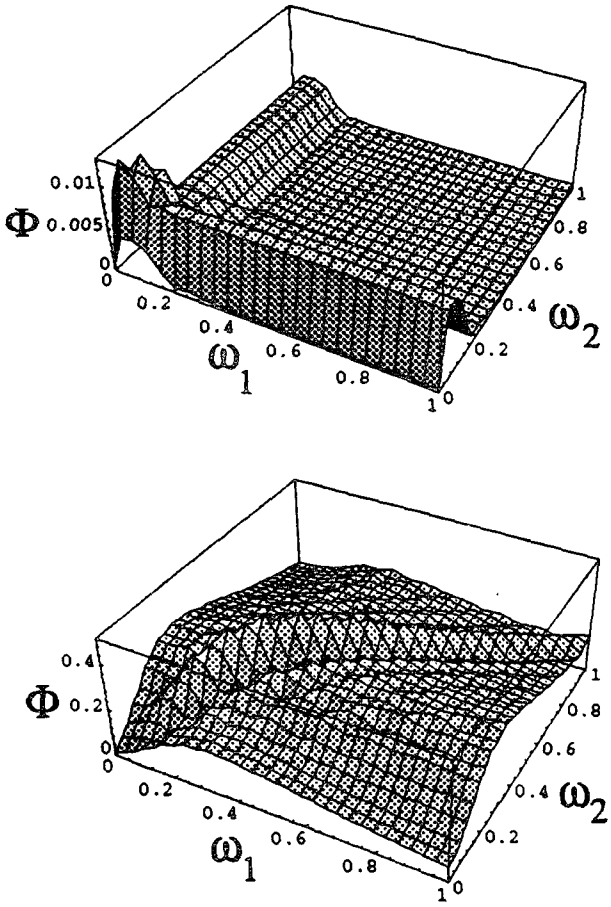

FIG. 6. Infinite-time flux as a function of ω_1 and ω_2 between R_1 and R_2 and between R_2 and R_3, respectively; $\delta_1 = \delta_{20} = 0$. The amplitudes satisfy $\gamma_1^2 + \gamma_2^2 = 1$ with $\gamma_1 = \sqrt{2}/3$.

average flux roughly gets smaller as both ω_1 and ω_2 are increased; see Fig. 9. One interesting phenomenon occurs for the transport across the boundary between R_2 and R_3, that is, the infinite-time average flux has a drop for ω_1 and ω_2 around 0.1. In the one-frequency case the flux is a strictly decreasing function of frequency (see Fig. 4 in Samelson 1992).

In Fig. 10 we plot the infinite-time averaged flux as a function of γ_1 and γ_2 with $\gamma_1^2 + \gamma_2^2 = 1$ and ω_1 fixed. We also see that the impact of two-frequency interference is complicated. The maximal flux across the boundary between R_2 and R_3 is much larger than that across the boundary between R_1 and R_2, while in the one-frequency case the maximal flux across both boundaries are almost the same (see Fig. 4 in Samelson 1992).

c. *A superimposed propagating wave train*

Following Samelson (1992), the nondimensional streamfunction for a superimposed propagating wave train is taken to be of the form

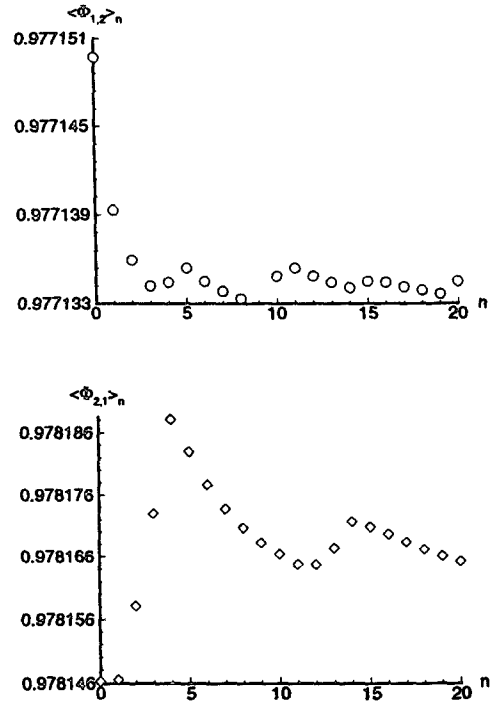

FIG. 7. Finite-time flux between R_1 and R_2; $\omega_1 = 0.3$, $\omega_2 = \pi$, $\gamma_1^2 + \gamma_2^2 = 1$ with $\gamma_1 = 0.5$, $\delta_1 = 3.5$, $\delta_{20} = \pi$.

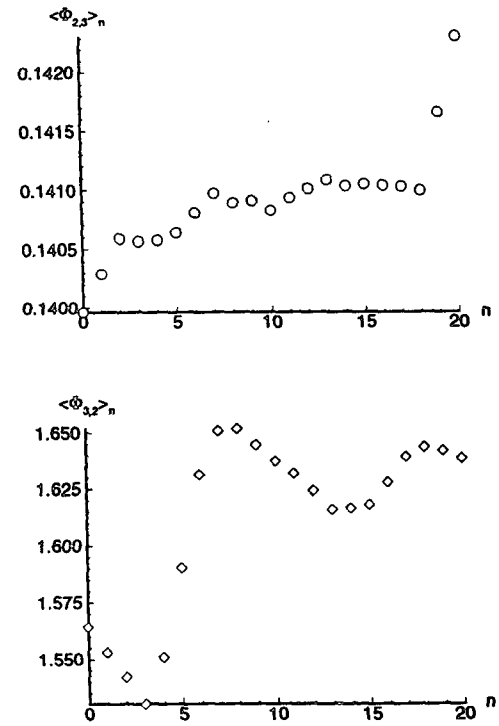

FIG. 8. Finite-time flux between R_2 and R_3; $\omega_1 = 0.3$, $\omega_2 = \pi$, $\gamma_1^2 + \gamma_2^2 = 1$ with $\gamma_1 = 0.5$, $\delta_1 = 3.5$, $\delta_{20} = \pi$.

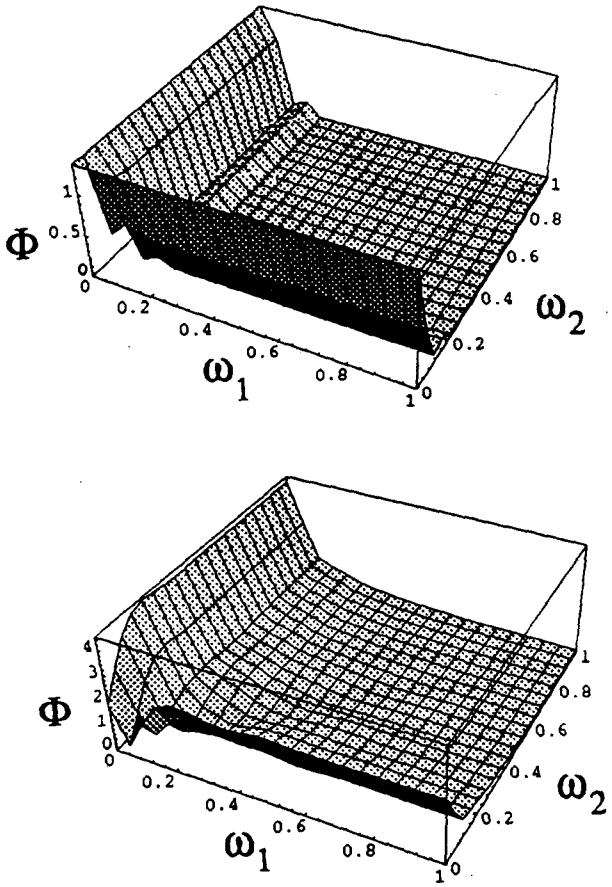

FIG. 9. Infinite-time flux as a function of ω_1 and ω_2 between R_1 and R_2 and between R_2 and R_3, respectively; $\delta_1 = \delta_{20} = 0$. The amplitudes satisfy $\gamma_1^2 + \gamma_2^2 = 1$ with $\gamma_1 = \sqrt{3}/2$.

$$\phi'(\xi, \eta, \tau) = \sum_{i=1}^{n} \gamma_i \frac{1}{p_i} \cos[p_i(\xi - c_{p_i}\tau) + \delta_i]. \quad (8)$$

1) PERIODIC VARIABILITY

For periodic variability of this type Samelson (1992) found that maximal values of exchange across the boundary between R_2 and R_3 were always larger than exchange across the boundary between R_1 and R_2. Moreover, he found that the exchange was greater if the propagating wave train phase speed was between the maximum and minimum (unperturbed) zonal velocities along the corresponding streamlines. For the boundary between R_1 and R_2 the nondimensional maximum and minimum basic flow zonal velocities are 0.0 and -0.1, respectively, and for the boundary between R_2 and R_3 they are 0.54 and 0.0, respectively (cf. Fig. 9 in Samelson 1992).

2) QUASIPERIODIC VARIABILITY AND THE COMPARISON WITH PERIODIC VARIABILITY

For two wave speed quasiperiodic variability of this type we show that the exchange process can be different from that observed by Samelson for periodic variability.

By arbitrarily fixing c_{p_1} and vary c_{p_2}, we compute infinite-time average fluxes across the boundaries between R_1 and R_2 and between R_2 and R_3. We compare the infinite-time average flux for two wave-speed case ($c_{p_1} \neq c_{p_2}$) and single-wave-speed case ($c_{p_1} = c_{p_2}$). We find that, for both boundaries, the infinite-time average flux for the two wave-speed case can either larger of smaller than for corresponding single wave-speed case.

We consider quasiperiodic variability with $p_1 = 2\pi$, $p_2 = \pi$, $\delta_1 = 0$, $\delta_{20} = 0$, and $\gamma_1^2 + \gamma_2^2 = 1$ with $\gamma_1 = 0.3$, while c_{p_1}, c_{p_2} are selected below.

For the boundary between R_1 and R_2, for example, we (arbitrarily) fix $c_{p_1} = -0.05$. The infinite-time average flux with wave speeds

$$(c_{p_1}, c_{p_2}) = (-0.05, -0.05), (-0.05, 0.2), (-0.05, -0.08)$$

are 0.59, 0.45, 1.47, respectively.

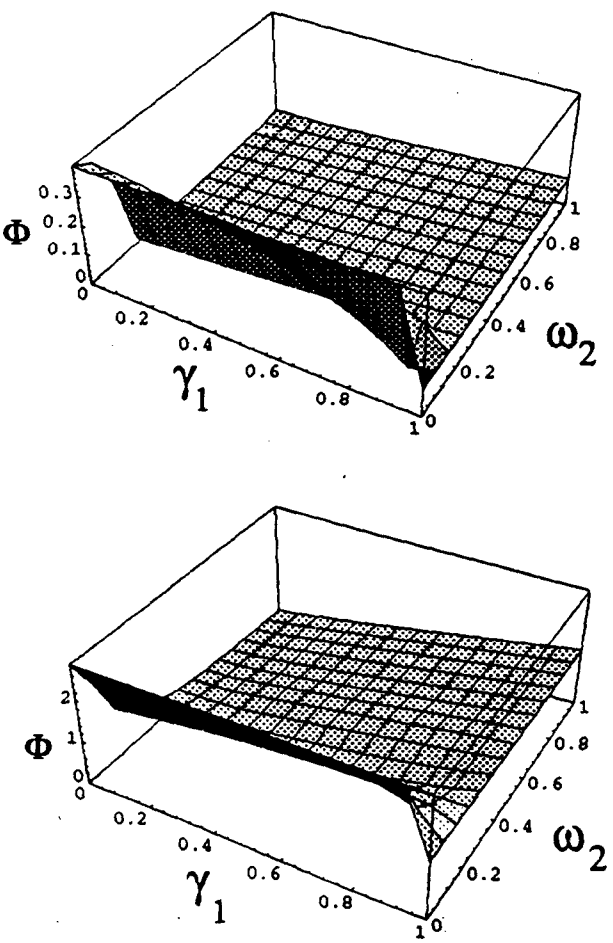

FIG. 10. Infinite-time flux as a function of γ_1 and ω_2, between R_1 and R_2 and between R_2 and R_3, respectively; $\omega_1 = 0.1$, $\gamma_1^2 + \gamma_2^2 = 1$, $\delta_1 = \delta_{20} = 0$.

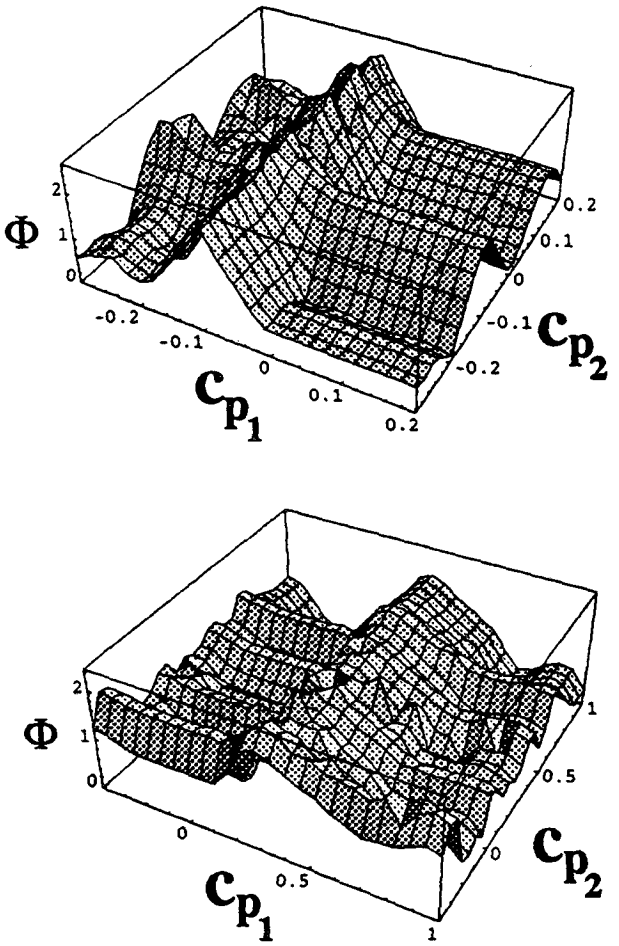

FIG. 11. Infinite-time flux as a function of c_{p_1} and c_{p_2} between R_1 and R_2 and between R_2 and R_3, respectively; $\gamma_1^2 + \gamma_2^2 = 1$ with $\gamma_1 = 0.3$, $\delta_1 = \delta_{20} = 0$, $p_1 = 2\pi/5$, $p_2 = \pi$.

For the boundary between R_2 and R_3, for example, we (arbitrarily) fix $c_{p_1} = 0.25$. The infinite-time average flux with wave speeds

$$(c_{p_1}, c_{p_2}) = (0.25, 0.25), (0.25, -0.15), (0.25, 0.19)$$

are 0.25, 0.09, 1.04, respectively.

In the one wave-speed case, relatively strong exchange is found to be confined in some interval of phase speed. However, in the two wave-speed case, the fluid exchange can be active outside such intervals (see Fig. 11). Moreover, the two wave speed perturbations tend to bring closer the maximal fluxes across the two boundaries as the difference between the maximal flux crossing the two boundaries are much smaller than that in the one wave-speed case (see Fig. 9 in Samelson 1992). This means that the two wave-speed interferences tend to balance the transport crossing the two boundaries. We note that this is very different from the case of the two previously considered two-frequency perturbations.

Acknowledgments. We would like to thank Darin Beigie for helpful discussions concerning the calculation of fluxes and Roger Samelson for many helpful suggestions. The computer programs used for the calculation of the different fluxes are available through the Caltech Control and Dynamical Systems anonymous ftp server. They can be obtained by using ftp and anonymously logging in to avalon.caltech.edu. They are in the directory /pub/cds/software under the titles *FiniteTimeFlux.ma* and *InfiniteTimeFlux.ma.* This research was supported by ONR Grant N00014-89-J-3023.

APPENDIX A

Transport in Quasiperiodically Time-Dependent Flows

The transport theory for quasiperiodically time varying vector fields is much more technical (as well as unfamiliar) than the case for time-periodic. Consequently, we will not present the theory in full mathematical generality but only develop the concepts necessary for the computations of fluxes and exchange rates in the meandering jet model. All of the theory in this appendix is developed and proved in Beigie et al. (1991, 1992) and Wiggins (1992).

We begin by considering a weakly quasiperiodically time-varying streamfunction of the following form

$$\psi(\xi, \eta, t; \epsilon) = \phi(\xi, \eta) + \epsilon\phi'(\xi, \eta, \omega_1 t, \cdots, \omega_l t; \mu, \epsilon), \quad \text{(A1)}$$

with the equations for fluid parcel trajectories given by

$$\dot{\xi} = -\frac{\partial\phi}{\partial\eta}(\xi, \eta) - \epsilon\frac{\partial\phi'}{\partial\eta}(\xi, \eta, \omega_1 t, \cdots, \omega_l t; \mu, \epsilon),$$

$$\dot{\eta} = \frac{\partial\phi}{\partial\xi}(\xi, \eta) + \epsilon\frac{\partial\phi'}{\partial\xi}(\xi, \eta, \omega_1 t, \cdots, \omega_l t; \mu, \epsilon), \quad \text{(A2)}$$

where each argument of ϕ' of the form $\omega_i t$ is periodic in t with period $2\pi/\omega_i$; $\mu \in \mathbb{R}^p$ denotes the possible parameters; and $0 < \epsilon \ll 1$ is a small dimensionless parameter. As an example, one could think of ϕ' as being composed of a finite sum of plane waves with different frequencies and relative phase differences, but we will see explicit examples shortly. If the frequencies are incommensurate, then the time dependence is not periodic, and therefore the Poincaré map formalism of dynamical systems theory and all of its attendant analytical tools cannot be applied.

We will handle this situation in a way that may appear rather strange at first, but we hope to remove this impression as we go along. We enlarge the phase space by introducing the phases of the different frequency components as new dependent variables to obtain the following equations for the parcel trajectories

$$\dot{\xi} = -\frac{\partial \phi}{\partial \eta}(\xi, \eta) - \epsilon \frac{\partial \phi'}{\partial \eta}(\xi, \eta, \delta_1, \cdots, \delta_l; \mu, \epsilon)$$

$$\dot{\eta} = \frac{\partial \phi}{\partial \xi}(\xi, \eta) + \epsilon \frac{\partial \phi'}{\partial \xi}(\xi, \eta, \delta_1, \cdots, \delta_l; \mu, \epsilon)$$

$$\dot{\delta}_1 = \omega_1$$

$$\vdots$$

$$\dot{\delta}_l = \omega_l. \qquad \text{(A3)}$$

Clearly, the $\xi - \eta$ components of (A3) are the same as (A2) since $\delta_i = \omega_i t + \delta_{i0}$.

The system is now an $l + 2$ dimensional *time-independent* set of equations. We can study the dynamics of this system via an $l + 1$ dimensional Poincaré map that is constructed in much the same spirit as in the case of time-periodic variability. Namely, rather than consider the evolution of continuous parcel trajectories in the full $l + 2$ dimensional phase space of this dynamical system, we plot their evolution at discrete intervals of time, where the interval of time is equal to the period of *one* of the frequency components of the variability (in the following we will assume that this distinguished frequency component is the lth, but any component can be taken into account in this manner just be relabeling the indices). We make this procedure more mathematically precise.

We construct the following $l + 1$ dimensional cross section, or *Poincaré section,* to the enlarged vector field (A3):

$$\Sigma^{\delta_{l0}} \equiv \{(\xi, \eta, \delta_1, \cdots, \delta_l) | \delta_l = \delta_{l0}\}. \qquad \text{(A4)}$$

The $l + 1$ dimensional Poincaré map of this cross section into itself is given by

$$P_\epsilon : \Sigma^{\delta_{l0}} \to \Sigma^{\delta_{l0}},$$

$$(\xi(0), \eta(0), \delta_1, \ldots, \delta_{l-1}) \mapsto \left(\xi\left(\frac{2\pi}{\omega_l}\right), \eta\left(\frac{2\pi}{\omega_l}\right),\right.$$

$$\left.\delta_1 + 2\pi \frac{\omega_1}{\omega_l}, \ldots, \delta_{l-1} + 2\pi \frac{\omega_{l-1}}{\omega_l}\right). \qquad \text{(A5)}$$

At this point, defining some new notation will make it much easier to write down subsequent formulas. The passage to the Poincaré map fixes the phase of one of the frequency components. We will lump the remaining $l - 1$ frequencies and phases into frequency and phase *vectors* defined respectively as follows:

$$(\omega_1, \ldots, \omega_{l-1}) \equiv \omega, \quad (\delta_1, \ldots, \delta_{l-1}) \equiv \delta.$$

The symbol μ represented external parameters in the problem. We can view the l frequencies as additional parameters and thus define a new parameter vector as follows:

$$\nu \equiv (\mu, \omega_1, \ldots, \omega_l).$$

Now we describe the advantages of recasting the original quasiperiodically time-dependent velocity field (A2) as a time-independent velocity field (A3) in a higher dimensional space. First of all, it provides a framework where we can study trajectories of this higher dimensional system via a Poincaré map, much as in the case for time periodic velocity fields. But more importantly, it provides a setting where we can understand the invariant manifold structure relevant for the problem of exchange across a meandering jet with quasiperiodic variability. Note that in the case where the variability only has a single frequency, the construction reduces to the standard two-dimensional Poincaré map.

We next consider the issues of "invariant manifold structure" in the context of this higher dimensional Poincaré map more carefully, and we motivate them from the point of view of perturbation of the steady flow. For $\epsilon = 0$ the δ components of (A3) decouple from the $\xi - \eta$ components (this is just a manifestation that the velocity field is steady for $\epsilon = 0$). Nevertheless, we can still view the invariant manifold structure of the steady velocity field (in particular, the stagnation points and the separatrices connecting them) in the enlarged $\xi - \eta - \delta$ space of the Poincaré section defined in (A4). In this case for each δ we have a "copy" of the steady two-dimensional stagnation point and streamline structure. Or, more mathematically, in the Poincaré section (A4) the stagnation points of the steady flow are manifested as the Cartesian product of the stagnation point in $\xi - \eta$ space with the $l - 1$ torus, T^{l-1} parametrized by the $l - 1$ angles denoted by δ. Similarly, the Cartesian product of the one-dimensional separatrices in the $\xi - \eta$ phase space with the $l - 1$ torus are manifested as l-dimensional surfaces in the $l + 1$ dimensional Poincaré section (A4); therefore, dimensionally they still act as separatrices in this higher dimensional space. To summarize in more mathematical terminology, in the higher dimensional Poincaré section obtained by including the phases of all the frequency components of the variability, for $\epsilon = 0$ the saddle-type stagnation point of the steady two-dimensional flow is manifested as a saddle-type $l - 1$ dimensional torus, which has l-dimensional stable and unstable manifolds that act as separating "tubes." We illustrate the geometry of this situation in Fig. A1.

For ϵ small, but nonzero, it can be shown that this saddle-type invariant torus along with its stable and unstable manifolds persists. However, now the l-dimensional stable and unstable manifolds of the saddle-type invariant torus need not coincide as in the steady case (i.e., for $\epsilon = 0$), but they may intersect in a very complicated geometrical fashion as illustrated in Fig. A2.

For fluid transport issues we are really only interested in the kinematics of the $\xi - \eta$ component of the Poincaré map, that is, in motion in the physical space of the fluid flow. We reconnect with this by considering

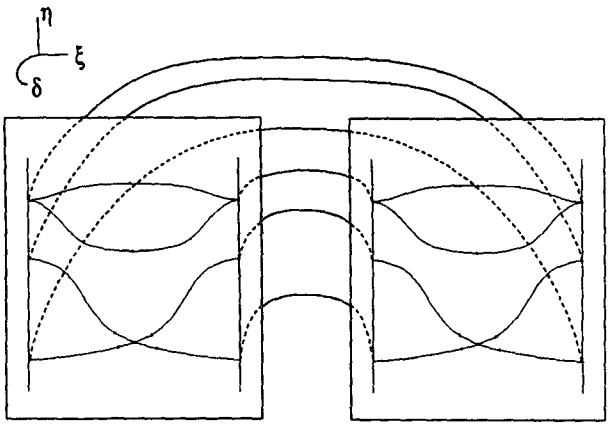

FIG. A1. The separatrix structure of the steady flow in the enlarged $\xi - \eta - \delta$ space (cut-away, one-half view).

the manifestation of these separating surfaces in appropriately defined two-dimensional *phase slices.* A two-dimensional phase slice of the $l + 1$ dimensional Poincaré section is defined as

$$\chi(\bar{\delta}) = \{(\xi, \eta, \delta, \delta_{l_0}) | \delta = \bar{\delta}\}. \qquad \text{(A6)}$$

Note that points on a phase slice are described by the coordinates $\xi - \eta$, which are the coordinates of the physical space of the fluid flow. Moreover, from (A5) we have

$$P_\epsilon\left(\chi\left(\delta + 2\pi m \frac{\omega}{\omega_l}\right)\right) = \chi\left(\delta + 2\pi(m+1)\frac{\omega}{\omega_l}\right), \qquad \text{(A7)}$$

or, in other words, phase slices map to phase slices, but with the defining phase of the original phase slice advanced by the phase vector $2\pi(\omega/\omega_l)$. The $l - 1$ dimensional saddle-type tori, along with their l dimensional stable and unstable manifolds, intersect each phase slices in points and curves, respectively. However, their location with respect to the coordinates on the phase slice (i.e., the physical space of the flow) may vary from phase slice to phase slice.

In this way the theory accounts for the spatial variation of the saddle-points along with their stable and unstable manifolds, as a result of the nonperiodic variability of the flow.

Now the strategy is much the same as it was in the case for the standard two-dimensional Poincaré map. On each phase slice we construct boundaries using segments of the stable and unstable manifolds of the tori. Associated with each boundary we construct turnstiles similar to the way that we did for the standard two-dimensional Poincaré map. For the case of weak variability there is a generalization of Melnikov's method to the quasiperiodic situation, and this tool enables us to carry out this program explicitly, as well as derive approximate analytical formulas for fluxes and exchange rates. In the following we will not carry out the geometrical construction of the "phase dependent" turnstiles explicitly. Instead, we will concentrate on deriving the approximate analytical formulas for fluxes and exchange rates. The quasiperiodic Melnikov function is given by

$$M(t_0, \delta; \nu, \delta_{l0}) = \int_{-\infty}^{+\infty} \{\phi, \phi'\}(\xi^h(t), \eta^h(t), \omega t + \omega t_0 + \delta, \omega_l t + \omega_l t_0 + \delta_{l0}, \nu, 0)dt, \qquad \text{(A8)}$$

where $(\xi^h(t), \eta^h(t))$ is a trajectory of the unperturbed problem connecting to saddle-type stagnation points, $\{\phi, \phi'\}$ is the *Poisson bracket* of ϕ with ϕ' defined by

$$\{\phi, \phi'\} = \frac{\partial\phi}{\partial\xi}\frac{\partial\phi'}{\partial\eta} - \frac{\partial\phi}{\partial\eta}\frac{\partial\phi'}{\partial\xi}, \qquad \text{(A9)}$$

and t_0 can be thought of as an arclength parameter along the unperturbed separatrix. On a fixed phase slice (i.e., for fixed δ), the quasiperiodic Melnikov function is a measure of the distance between the stable and unstable manifolds measured along a line perpendicular to the unperturbed separatrix at the point parameterized by t_0 on the phase slice $\chi(\delta)$ (δ_{l0} is the phase that is fixed in defining the Poincaré section).

We now discuss transport due to quasiperiodic variability across the upper boundary of the jet between the northern recirculation cell (R_2) and the northern retrograde regime (R_1). Suppose at $t = 0$ the phases of all the frequency components of the variability are given by (δ, δ_{l0}), and consider a phase slice

$$\chi\left(\delta + 2\pi m \frac{\omega}{\omega_l}\right).$$

Let $t_0(\delta + 2\pi m(\omega/\omega_l))$ denote a simple zero of the quasiperiodic Melnikov function restricted to this phase slice that is the parameter value corresponding to our chosen boundary intersection point on this phase slice. Then the segments of the stable and unstable manifolds

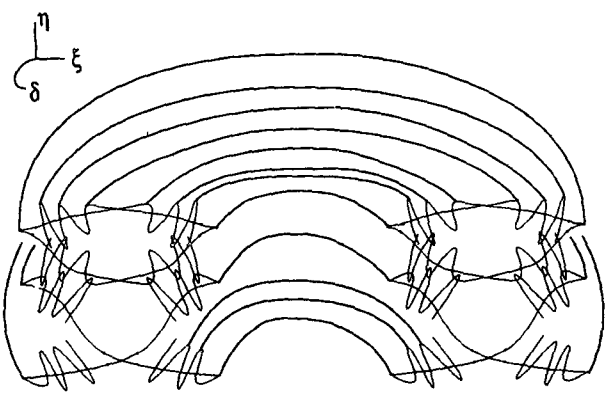

FIG. A2. The separatrix structure of the unsteady flow in the enlarged $\xi - \eta - \delta$ space (cut-away, one-half view).

"beginning" on the intersection of the saddle points and ending at this boundary intersection point form a boundary. We label the regions on each sides of the boundary by $R_1(\delta + 2\pi m(\omega/\omega_l))$ and $R_2(\delta + 2\pi m(\omega/\omega_l))$, as shown in Fig. A3 and Fig. A4.

This construction can be carried out on any phase slice. So consider the phase slice

$$\chi\left(\delta + 2\pi(m+1)\frac{\omega}{\omega_l}\right)$$

with the point

$$t_0\left(\delta + 2\pi(m+1)\frac{\omega}{\omega_l}\right)$$

analogously defined. Then let $t_0^{-1}(\delta + 2\pi m(\omega/\omega_l))$ denote the parameter corresponding to the preimage under the Poincaré map P_ϵ of the point on

$$\chi\left(\delta + 2\pi(m+1)\frac{\omega}{\omega_l}\right)$$

parameterized by

$$t_0\left(\delta + 2\pi(m+1)\frac{\omega}{\omega_l}\right).$$

From (A7), this point is on the phase slice $\chi(\delta + 2\pi m(\omega/\omega_l))$. The lobes between the points parameterized by $t_0(\delta + 2\pi m(\omega/\omega_l))$ and $t_0^{-1}(\delta + 2\pi m(\omega/\omega_l))$ form the turnstile lobes; see Fig. A2. Between adjacent zeros the sign of the quasiperiodic Melnikov function will be constant. Using this, combined with the geometrical meaning of the Melnikov function as a

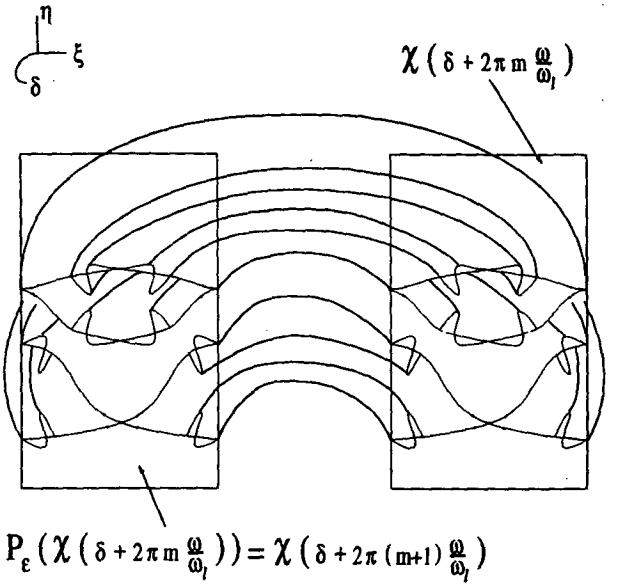

FIG. A3. Boundaries and turnstiles in the enlarged $\xi - \eta - \delta$ space (cut-away, one-half view).

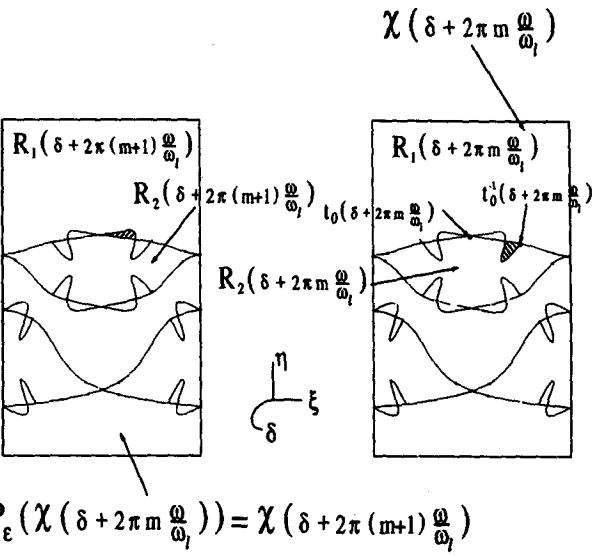

FIG. A4. Boundaries and turnstiles on subsequent phase slices. Hatched lobes map to hatched lobes.

signed distance measurement (see Wiggins 1992), we can determine whether or not a lobe is in $R_1(\delta + 2\pi m(\omega/\omega_l))$ or $R_2(\delta + 2\pi m(\omega/\omega_l))$ on the phase slice $\chi(\delta + 2\pi m(\omega/\omega_l))$. For $\nabla\phi$ having the direction shown in Fig. 1 we have

$$M\left(t_0, \delta + 2\pi m\frac{\omega}{\omega_l}; \delta_{10}\right)$$

$$\begin{cases} >0 \Rightarrow \text{lobe in } R_1\left(\delta + 2\pi m\dfrac{\omega}{\omega_l}\right) \\ <0 \Rightarrow \text{lobe in } R_2\left(\delta + 2\pi m\dfrac{\omega}{\omega_l}\right). \end{cases}$$

The *instantaneous flux from* $R_i(\delta + 2\pi m(\omega/\omega_l))$ *into* $R_j(\delta + 2\pi(m+1)\omega/\omega_l)$ is given by

$$\Phi_{i,j}(m) \equiv \frac{\omega_l}{2\pi} \times \left\{ \begin{array}{l} \text{the area in } R_i\left(\delta + 2\pi m\dfrac{\omega}{\omega_l}\right) \text{ that moves into} \\ \qquad R_j\left(\delta + 2\pi(m+1)\dfrac{\omega}{\omega_l}\right) \text{ in one iterate} \end{array} \right\}. \tag{A10}$$

Note that in general $\Phi_{1,2}(m) \neq \Phi_{2,1}(m)$ and that $\Phi_{i,j}(m)$ depends on δ. The instantaneous flux can be calculated approximately from the quasiperiodic Melnikov function. Defining the positive and negative parts of the Melnikov function as follows:

$$M^+ = \max(M, 0)$$
$$M^- = -\min(M, 0),$$

we have

$$\Phi_{1,2}(m) = \epsilon\left|\int_{t_0^{-1}(\delta+2\pi m(\omega/\omega_l))}^{t_0(\delta+2\pi m(\omega/\omega_l))} M^+\left(t_0, \delta + 2\pi m\frac{\omega}{\omega_l}; \delta_{l0}\right)dt_0\right| + O(\epsilon^2). \quad \text{(A11)}$$

Here $\Phi_{2,1}(m)$ can be calculated from (A11) by replacing M^+ with M^- in the expression. *Finite-time average flux* is defined as

$$\langle\Phi_{i,j}\rangle_n = \frac{1}{n+1}\sum_{m=0}^{n}\Phi_{i,j}(m), \quad \text{(A12)}$$

where, also, in general, $\langle\Phi_{1,2}\rangle_n \neq \langle\Phi_{2,1}\rangle_n$ and $\langle\Phi_{i,j}\rangle_n$ depend on δ. Finally, the *infinite-time average flux* is given by

$$\langle\Phi_{1,2}\rangle = \langle\Phi_{2,1}\rangle = \lim_{n\to\infty}\frac{1}{n+1}\sum_{m=0}^{n}\Phi_{1,2}(m). \quad \text{(A13)}$$

Thus, for a given boundary there are *five* different fluxes associated with the boundary.

Flux formulas for transport between any two adjacent regions are computed in exactly the same way. The only difference is that the quasiperiodic Melnikov function used in the formulas is computed along the unperturbed separatrix that is the boundary between the regions.

For the case of time-periodic variability $\delta = 0$, that is, there are no phase slices on the Poincaré section (or, alternatively, the Poincaré section is the phase slice, and it is mapped back into itself by the Poincaré map). In this situation it is easy to show that $\Phi_{1,2}(m) = \Phi_{2,1}(n)$ for all n, m from which it follows that

$$\Phi_{1,2}(n) = \Phi_{2,1}(n) = \langle\Phi_{1,2}\rangle_n = \langle\Phi_{2,1}\rangle_n = \langle\Phi_{1,2}\rangle = \langle\Phi_{2,1}\rangle.$$

This is another indication that transport and exchange for quasiperiodic variability may be very different than for the case of periodic variability.

APPENDIX B

The Form of the Quasiperiodic Melnikov Functions for the Three Different Types of Variability

In this appendix we derive the form of the quasiperiodic Melnikov functions for the three different types of variability discussed earlier.

a. Quasiperiodically time-varying meander amplitude

For this streamfunction the quasiperiodic Melnikov functions can now be computed. Using (A8), (A9), and some trigonometric identities we obtain

$$\begin{aligned}M(\tau_0, \delta, \delta_{l0}) &= \sum_{i=1}^{l-1}\gamma_i A_1(\omega_i)\cos(\omega_i\tau_0 + \delta_i) \\ &+ \sum_{i=1}^{l-1}\gamma_i A_2(\omega_i)\sin(\omega_i\tau_0 + \delta_i) \\ &+ \sum_{i=1}^{l-1}\gamma_i B_1(\omega_i)\cos(\omega_i\tau_0 + \delta_i) \\ &+ \sum_{i=1}^{l-1}\gamma_i B_2(\omega_i)\sin(\omega_i\tau_0 + \delta_i) + \gamma_l A_1(\omega_l) \\ &\times\cos(\omega_l\tau_0 + \delta_{l0}) + \gamma_l A_2(\omega_l)\sin(\omega_l\tau_0 + \delta_{l0}) \\ &+ \gamma_l B_1(\omega_l)\cos(\omega_l\tau_0 + \delta_{l0}) \\ &+ \gamma_l B_2(\omega_l)\sin(\omega_l\tau_0 + \delta_{l0}), \quad \text{(B1)}\end{aligned}$$

where

$$\begin{aligned}A_1(\omega_i) &\equiv \int_{-\infty}^{+\infty}\left(\frac{\partial\phi}{\partial\xi}\frac{\partial\phi}{\partial\eta\partial B}\right)\cos\omega_i\tau d\tau \\ A_2(\omega_i) &\equiv -\int_{-\infty}^{+\infty}\left(\frac{\partial\phi}{\partial\xi}\frac{\partial\phi}{\partial\eta\partial B}\right)\sin\omega_i\tau d\tau \\ B_1(\omega_i) &\equiv -\int_{-\infty}^{+\infty}\left(\frac{\partial\phi}{\partial\eta}\frac{\partial\phi}{\partial\xi\partial B}\right)\cos\omega_i\tau d\tau \\ B_2(\omega_i) &\equiv \int_{-\infty}^{+\infty}\left(\frac{\partial\phi}{\partial\eta}\frac{\partial\phi}{\partial\xi\partial B}\right)\sin\omega_i\tau d\tau. \quad \text{(B2)}\end{aligned}$$

The form of the quasiperiodic Melnikov function can be simplified as follows:

$$\begin{aligned}M(\tau_0, \delta, \delta_{l0}) &= \sum_{i=1}^{l-1}\gamma_i M_0(\omega_i)\cos(\omega_i\tau_0 + \delta_i - \alpha_i) \\ &+ \gamma_l M_0(\omega_l)\cos(\omega_l\tau_0 + \delta_{l0} - \alpha_l), \quad \text{(B3)}\end{aligned}$$

where

$$M_0(\omega_i) = \sqrt{(A_1(\omega_i) + B_1(\omega_i))^2 + (A_2(\omega_i) + B_2(\omega_i))^2} \quad \text{(B4)}$$

and

$$\alpha_i = \tan^{-1}\left(\frac{A_2(\omega_i) + B_2(\omega_i)}{A_1(\omega_i) + B_1(\omega_i)}\right). \quad \text{(B5)}$$

For studying exchange between the northern recirculation cell (R_2) and the northern retrograde region (R_1), the integrands in (B2) are evaluated along the *unperturbed* separatrix that is the boundary between these regions, and in studying exchange between the jet core (R_3) and the northern recirculation cell (R_2) the integrands in (B2) are evaluated along the unperturbed separatrix that is the boundary between these regions.

We do not believe that (B2) can be computed analytically for this problem; however, they can be computed very easily via numerical integration. With the Melnikov function in hand, the approximate exchange rates can be calculated using the flux formulas given in (A11), (A12), and (A13).

b. A superimposed quasiperiodically time-varying spatially uniform meridional flow

From the same calculations as above, the quasiperiodic Melnikov function for this variability has the form

$$M(\tau_0, \delta, \delta_{l0}) = \sum_{i=1}^{l-1} \gamma_i M_0(\omega_i) \cos(\omega_i \tau_0 + \delta_i - \alpha_i) + \gamma_l M_0(\omega_l) \cos(\omega_l \tau_0 + \delta_{l0} - \alpha_l), \quad \text{(B6)}$$

where

$$M_0(\omega_i) = \sqrt{C_1(\omega_i)^2 + C_2(\omega_i)^2}$$

$$\alpha_i = \tan^{-1}\left(\frac{C_2(\omega_i)}{C_1(\omega_i)}\right)$$

$$C_1(\omega_i) = -\int_{-\infty}^{+\infty} \frac{\partial \phi}{\partial \eta} \cos\omega_i \tau d\tau$$

$$C_2(\omega_i) = -\int_{-\infty}^{+\infty} \frac{\partial \phi}{\partial \eta} \sin\omega_i \tau d\tau.$$

The coefficients $C_1(\omega_i)$ and $C_2(\omega_i)$ are evaluated along the unperturbed separatrices that are appropriate for the exchange problem being considered. As in the previous case, the amplitudes of the Melnikov functions can easily be computed numerically, and the resulting Melnikov functions can then be used to compute the approximate exchange rates using the flux formulas given in (A11), (A12), and (A13).

c. A superimposed propagating wave train

From the same calculations as in the previous two cases, the quasiperiodic Melnikov function for this variability has the form

$$M(\tau_0, \delta, \delta_{l0}) = \sum_{i=1}^{l-1} \gamma_i M_0(\omega_i) \cos(p_i c_{p_i} \tau_0 - \delta_i - \alpha_i) + \gamma_l M_0(\omega_l) \cos(p_l c_{p_l} \tau_0 - \delta_{l0} - \alpha_l), \quad \text{(B7)}$$

where

$$M_0(\omega_i) = \sqrt{D_1(\omega_i)^2 + D_2(\omega_i)^2}$$

$$\alpha_i = \tan^{-1}\frac{D_2(\omega_i)}{D_1(\omega_i)}$$

$$D_1(\omega_i) = \int_{-\infty}^{+\infty} \frac{\partial \phi}{\partial \eta} \sin(p_i(\xi - c_{p_i}\tau))$$

$$D_2(\omega_i) = -\int_{-\infty}^{+\infty} \frac{\partial \phi}{\partial \eta} \cos(p_i(\xi - c_{p_i}\tau)).$$

As before, the coefficients $D_1(\omega_i)$ and $D_2(\omega_i)$ are evaluated along the unperturbed separatrices that are appropriate for the exchange problem being considered. As in the previous cases, the amplitudes of the Melnikov functions can easily be computed numerically, and the resulting Melnikov functions can then be used to compute the approximate exchange rates using the flux formulas given in (A11), (A12), and (A13).

REFERENCES

Beigie, D., A. Leonard, and S. Wiggins, 1991: Chaotic transport in the homoclinic and heteroclinic tangle regions of quasiperiodically forced two dimensional dynamical systems. *Nonlinearity,* **4,** 775–819.

——, ——, and ——, 1992: The dynamics associated with the chaotic tangles of two-dimensional quasiperiodic vector fields: Theory and applications. *Nonlinear Phenomena in Atmospheric and Oceanic Sciences, IMA Volumes in Mathematics and its Applications,* Vol. 40. G. F. Carnevale, and R. Pierrehumbert, Eds., Springer-Verlag, 47–138.

——, ——, and ——, 1994: Invariant manifold templates for chaotic advection. *Chaos, Solitons, Fractals,* **4,** 749–868.

Bower, A. S., 1991: A simple kinematic mechanism for mixing fluid parcels across a meandering jet. *J. Phys. Oceanogr.,* **21,** 173–180.

Ottino, J., 1989: *The Kinematics of Mixing: Stretching, Chaos, and Transport.* Cambridge University Press, 364 pp.

Samelson, R. M., 1992: Fluid exchange across a meandering jet. *J. Phys. Oceanogr.,* **22,** 431–440.

Wiggins, S., 1990: *Introduction to Applied Nonlinear Dynamical Systems and Chaos.* Springer-Verlag, 672 pp.

——, 1992: *Chaotic Transport in Dynamical Systems.* Springer-Verlag, 301 pp.